EXPERIMENTAL STUDY OF TAIL ROTOR-FIN INTERFERENCE RATIO IN HOVER

Elmar Recker, Florian Pandele
Royal Military Academy
Rue de la Renaissance 30, Brussels, 1000
Belgium

Abstract

The paper presents an experimental study of tail rotor and fin interference in hover and in the absence of a main rotor. A high and a ventral/dorsal low tail design are investigated on a model rotor. For the high tail conception in tractor configuration previous observations are substantiated. By contrast, in pusher configuration, besides early-identified factors the direction of rotation and tail rotor longitudinal position appear to control the interference. Accordingly a widened parametric model is proposed. The connected power increment, observed to scale with the thrust interference ratio, completes the description. For the low tail conception, on the one hand, low values of the fin/rotor separation distance are seen to handicap adequate thrust interference ratios as compared to the high tail constellation. On the other hand, with growing tail rotor/fin spacing, a substantial gain shows up. Finally, the ventral/dorsal arrangement is seen to benefit from a slightly improved power required.

1. INTRODUCTION

The vast majority of helicopters in production are of the single main rotor with tail rotor configuration. The primary purpose of the tail rotor is twofold. First, the tail rotor provides an antitorque force to counter the torque reaction of the main rotor on the fuselage. Second, the tail rotor gives yaw stability and must provide the specified yaw acceleration in the maximum specified crosswind conditions. While the tail rotor itself provides considerable yaw stability, a vertical stabilizer may also be required to provide sufficient aerodynamic side force to offset the tail rotor thrust in forward flight and to provide sufficient antitorque to allow continued flight in the event of the loss of tail rotor. Aerodynamic interference effects between the tail rotor and the vertical fin tend to reduce the net thrust and to increase the power required for the rotor. Early studies [1], [2] identified the tail rotor type of installation, tractor and pusher, the fin/rotor separation distance and fin area/disc area as major parameters. The interaction penalties are reported smallest for pusher tail rotors, large fin/tail rotor separation distances within weight restrictions and fin/tail blockage ratios as small as possible. In addition to the placement of the tail rotor with respect to the fin, the designer is faced not all-inclusively with noise, handling qualities, safety, drive system complexity and main rotor/tail rotor interference considerations. To minimize noise the tail rotor vertical location should be low [3] and a bottom forward (BF) sense of rotation is advised [4]. According to [2] a bottom forward (BF) direction of rotation and raised position [5] is tailored to minimize the thrust fluctuations and pedal excursions during sideward flight when operating in the vortex ring state. Supplementary reason for selecting a high tail rotor vertical location is a less significant lateral tilt in hover [6] and enhanced ground clearance. In contrast to enhanced stability and safety characteristics, on the one hand, a vertical fin top installed tail rotor results in higher weight and complexity. On the other hand, a tail rotor positioned in the main rotor plane or in close proximity features the greatest main rotor power penalty [3], whereas the level of tail rotor power required is lowest [2]. Cognizant of the conflicting design options a wide variety of vertical fin and tail rotor combinations is found in single main rotor with tail rotor helicopter conceptions. A generic overview is given in Table 1. In general, the tail rotor centreline of rotation averages 1.1 times the tail rotor radius (R) aft of the main rotor blade tip, the vertical spacing varies from about $0.5\,R$ above the plane of the main rotor to about $1.4\,R$ below, the fin/tail rotor area ratios (S/A) range approximately from 0.2 to 0.4 and the vertical fin/tail rotor separation distances adimensionalised by R (x/R) are close to 0.3 – 0.5. However preferred configurations come out. First, heavy weight helicopters typically have a high tail on a sole dorsal vertical fin giving a low fin to disc are ratio, while in the contrary low weight helicopters predominantly feature a tail rotor at boom height on a combined dorsal and ventral vertical fin construct and taking advantage of an enlarged fin/rotor separation distance by placing the vertical fin boom off centre on a regular basis. Second, BF rotating tail rotors prevail. Finally, pusher installations are larger in number. Other than the commonalities no systematic longitudinal tail rotor position on the vertical fin shows up.

Design existing helicopter								
Installation	Pusher	Pusher	Tractor	Pusher	Pusher	Pusher	Pusher	Pusher
Separation distance [1]	0.32	0.38	0.40	0.40	0.43	0.49	0.48	0.52
Disc to fin area ratio [1][2]	0.18	0.22	0.2	0.2	0.4	0.42	0.38	0.3
Tail rotor position with respect to fin	High Mid	High Fore	High Fore	High Aft	Low Fore	Low Mid	Low Aft	Low Mid
Vertical fin position with respect to boom	Centre	Centre	Centre	Centre	Centre	Off centre	Off centre	Off centre
Direction of rotation	BF	BF	BF	BF	BF	BF	BA	BA

[1] Separation distance and Disc to fin area ratio are estimates
[2] Blockage area combines boom and vertical fin

Table 1: Physical tail rotor boom conception characteristics of existing helicopters.

Although extensive design guidelines are given in [2], to the authors' best knowledge the tail rotor sense of rotation, BF vs bottom aft (BA) and the longitudinal location on the vertical fin, fore, mid or aft, have been discarded in tail rotor/vertical fin aerodynamic interference studies up to date. The paper looks into the impact of those two distinct features on the thrust interference ratio

$$(1) \qquad F/T = 1 - T_{T_{net}}/T_{T_{req.}},$$

where $T_{T_{net}}$ and $T_{T_{req.}}$ are the tail rotor net thrust in presence of the fin and the required thrust produced by the tail rotor in absence of the vertical fin, by experimenting a high and low tail representative design in hover without main rotor interference. Besides the new parameters, the longitudinal position and rotational sense, the study includes the former observed factors, pusher vs tractor, x/R and S/A. The F/Ts are complemented by the associated power increment

$$(2) \qquad P_{ratio} = P_{T_{net}}/P_{T_{req.}}.$$

The paper is organized as follows. The experimental technique is addressed in Section 2. The model rotor and fin layouts are qualified, the rotor flow topology and performance are characterized and the experimental set-up is described. The results, addressing the high and low rotor concept, are presented in Section 3. Finally conclusions are drawn in Section 4.
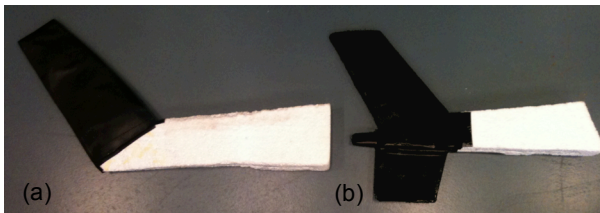

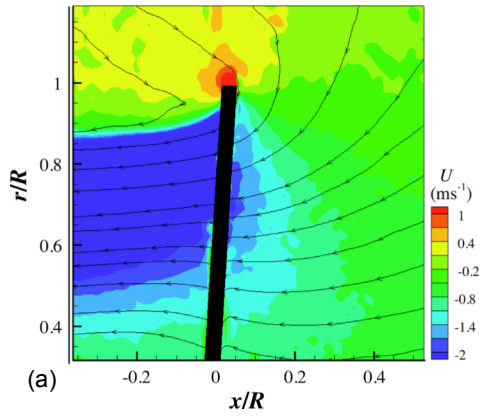Fig. 1: Photographic view of the model fin conception: (a) High tail; (b) Low tail

2. EXPERIMENTAL TECHNIQUE
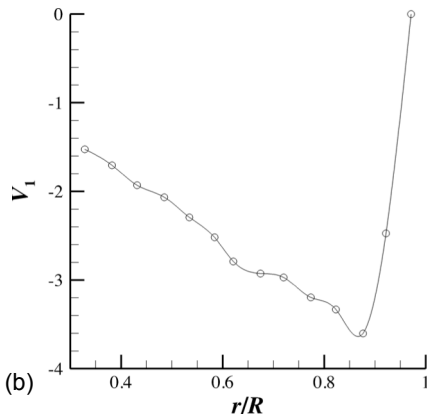
2.1. Model rotor and fin layouts

The rotor and rotor head used are derived from the Graupner model helicopter Micro Star 400. The miniature electrical helicopter is particularized by an approximate all-up weight of 5 N and a rotor reduction ratio of 8.25. Originally the rotor head consists of a flybar for cyclic and a two bladed main rotor for collective control. Departing from the baseline rotor hub, the flybar was removed and the main rotor pitch control was maintained only. The collective pitch (θ) ran from −7 to 18°. The main rotor blades are basically characterized by $R = 312$ mm, a constant chord of 32.3 mm, no twist, leading edge sweep at the blade tip, a 6 cm root cut-out and a NACA0012 alike symmetrical airfoil. Accordingly the solidity ratio $\sigma = 0.066$. A photographic view of the installed rotor, rotor head and assembly is given in Fig. 4(b). The fin section was made of Polystyrene covered by a plastic film (Fig. 1). A typical high (Fig. 1(a)) and low fin conception (Fig. 1(b)) was scaled to representative S/As leading to an approximate $A = 0.11$ m^2.

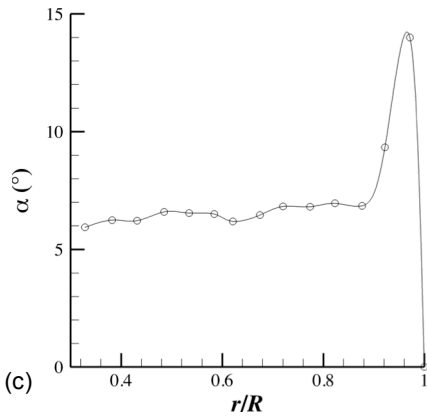### 2.2. Flow topology and performance

To qualify the flow through the reduced size rotor and to link up the flow behavior to actual rotors, the flow through the miniature rotor was investigated by two-dimensional Particle Image Velocimetry recording the in-plane components of the instantaneous velocity vector. The air was seeded with oil droplets (1 − 3 µm). Image pairs were recorded with an acquisition rate of 15 Hz. 500 image pairs were recorded. The interrogation region was 32×32 pixels and was shifted 16 pixels (50% overlap) for each data point. Peak and moving average validation were applied for removing outliers. After post-processing, the validated vector maps were temporally averaged. The laser sheet

(a)

(b)

(c)

Fig. 2: Flow topology: (a) Averaged axial velocity U ($\theta = 7°$, $\Omega = 1,300$ rpm); (b) Averaged induced velocity V_1 ($\theta = 14°$, 1,000 rpm); (c) Averaged local angle of attack α (Operating conditions as in (b))

has been positioned on a plane containing the rotational axis. The image size in physical dimensions was approximately 50×35cm, yielding a spatial resolution of about 1cm. The averaged axial velocity component U is represented in Fig. 2(a) for $\theta = 7°$ and a rotational speed $\Omega = 1,300$ rpm. In line with smoke visualizations by [7], the rotor wake contracts from the diameter of the rotor to its remote wake size in about a third of the rotor radius. What is more, the rotor is seen to suck in air from underneath the rotor plane. The condition at the rotor is quantified through the averaged vertical
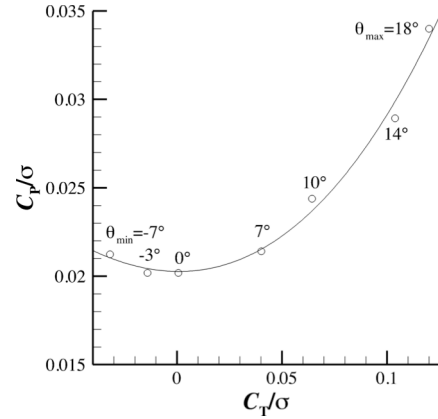

Fig. 3: Rotor performance

induced velocity (V_1) (Fig. 2(b)) and the local angle of attack (α) (Fig. 2(c)) computed from

(3) $$\alpha = \theta + V_1/\Omega r,$$

where r is the radial station. The induced velocity was obtained by probing U radially 5 mm downstream of the rotor plane. The operating conditions were set at $\theta = 14°$ and $\Omega = 1,000$ rpm. On the one hand, in Fig. 2(b) the averaged vertical induced velocity is seen to go to zero around $0.97\,R$. On the other hand, the experimental clockwise curvature of V_1, in contrast to the counterclockwise theoretical curvature, and the large discontinuities in the angle of attack distribution near the blade tip observed in Fig. 2(c) are the trace of tip vortex interaction. Similar in flow behavior to full-scale helicopter experiments [8] and computations [9], the miniature rotor is regarded suitable for the use of analyzing tail rotor/fin interference. The performance of the small-scale rotor is shown in Fig. 3, plotting the non-dimensional power coefficient C_P/σ against the thrust coefficient C_T/σ. The reader is referred to Section 2.3 for the determination of the power P and the thrust T to calculate C_P/σ and C_T/σ respectively. Although the general evolution correlates well with actual rotor geometries [10], the zero lift C_P/σ is 10 order of magnitudes larger than the full-scale counterpart [10]. The difference originates in the zero lift drag coefficient (C_{D_0}) dependency on the Reynolds number (Re). Tail rotors typically operate at Re from 2×10^6 to 6×10^6, while model rotors are restricted to $Re = 3\times10^6$. The test specific Re is elaborated in Section 2.3. Even so, as the experimental study gives no attention to absolute values, but focuses on T and P ratios, exporting the small-scale properties to full-scale rotors is considered adequate.

2.3. Experimental set-up

The measuring chain is visualized in Fig. 4. The model rotor was driven by an electric drill. To
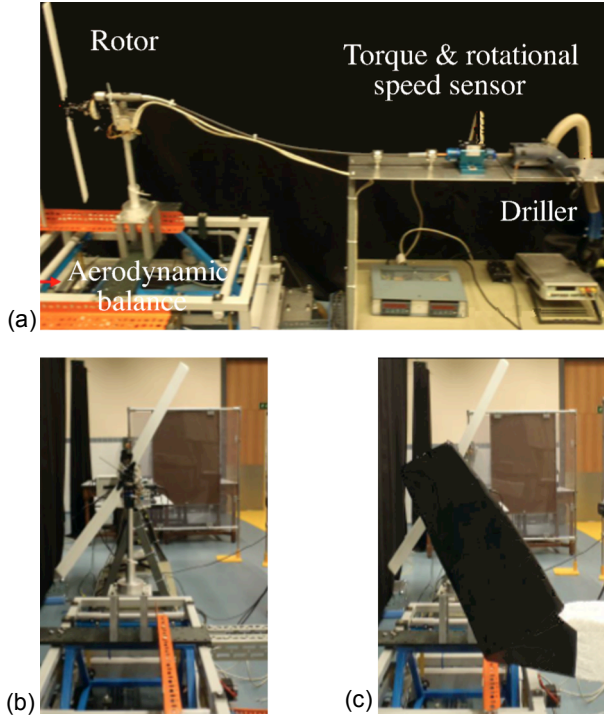
Fig. 4: Experimental set-up: (a) Measuring chain side view; (b) Fin-less end view; (c) High tail pusher/BA end view

compute P, the rotational speed and torque Q were sensed by a rotational speed and torque sensor. The measurings range were respectively Ω = 12,000 rpm and Q = 2 Nm with an accuracy of <0.1% full scale. The thrust was measured by an independent 3-component underfloor aerodynamic balance characterized by a maximal longitudinal force of 75 N and an accuracy of <0.1% full scale. To work out F/T (Equation (1)), $T_{T_{net}}$ and $T_{T_{req.}}$ were quantified at equal power, specified by Ω = 1,000 rpm and the blade pitch set at θ_{max} = 18°. The operational point corresponded to C_P/σ = 0.034 on Fig. 3. The comparatively low Ω for model helicopter application was conditioned by the torque sensor maximum rotational speed and the rotor head speed reduction, resulting in $Re \approx$ 70,000 with the blade chord and tip speed as characteristic length and velocity respectively. As such the

$x/R = [0.40, 0.46, 0.53, 0.59, 0.65]$

Fig. 5: Experimental condition schematic view: (a) High tail; (b) Low tail

relatively large C_P/σ at zero thrust is substantiated. The power ratio (Equation (2)) was evaluated at equal Ts corresponding to C_T/σ = 0.12 (Fig. 3). The blade pitch was kept constant at θ_{max} and the reduction in $T_{T_{net}}$ by the fin/rotor interference was compensated for by varying Ω. A schematic drawing of the test pattern is shown in Fig. 5. For the high tail model (Fig. 5(a)) five equally spaced test points at the fin leading (1 – 5) and trailing edge (1' – 5') were experimented. Three longitudinally spaced points centred on the boom (11 – 13) were taken into consideration for the low tail design (Fig. 5(b)). The fin/rotor separation distance ranged from 0.40 to 0.65. Although x/Rs down to 0.30 are common in helicopter design (Table 1), due to significant blade coning, a higher lower limit was set to avoid rotor/fin strike. Representative S/As spanning from 0.18 – 0.42 were made possible by the fin/rotor scaling. In the first place the direction of rotation was set to BA. Secondarily BF direction of rotation was looked into for the high tail points free of fin/boom obstruction (1 – 3, 1' – 3'), as schematized by the dashed rotor circumference in Fig. 5(a). Pusher and tractor installations were investigated alternately for the high tail constellation. The low tail experimentation effort was limited to a pusher arrangement. Thrust interference investigations were conducted for all concepts. The associated power increments were determined for the high tail pusher and low tail set-up only. The test matrix is summarized in Table 2. As an illustration an end-view of the experimental apparatus for the fin-less and high tail pusher/BA measurements are depicted in Figs. 4(b) and (c).

Conception	High			Low
Position	1 - 5 1' - 5'	1 - 3 1' - 3'	1 - 5 1' - 5'	11 - 13
Installation	Pusher		Tractor	Pusher
Rotation sense	BA	BF	BA	BA
F/T	✓	✓	✓	✓
x/R and S/A	See Fig. 5			
P_{ratio}	✓			✓

Table 2: Experimental test matrix

3. RESULTS

The results are presented as follows. First, in Section 3.1, the focus is on the high tail rotor concept. Consecutively F/T and P_{ratio} are looked into, a combined model is proposed and a design guideline is given. Second, F/T and P_{ratio} for the low tail rotor concept are analyzed in Section 3.2 and compared to the high tail findings in Section 3.3. Section 3.3 concludes with the potential towards
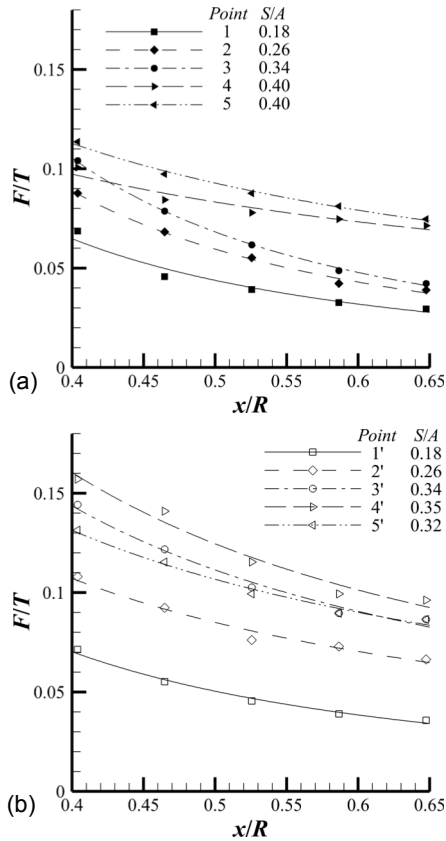
Fig. 6: High tail pusher/BA F/T: (a) leading edge; (b) trailing edge

optimization for ventral/dorsal low tail rotor design as compared to undivided high fin layouts.

3.1. High tail rotor concept

3.1.1. Thrust interference

Both, the leading and trailing edge locations, F/Ts for the pusher installation and BA rotational direction are presented in line in Fig. 6. In general an alike [1] overall dependence of F/T on x/R and S/A is observed for points 1 – 3 and 1' – 5' (see Fig. 5(a) for location reference); the thrust interference effects are seen to be minimized at large x/Rs and small S/As. More specific, first, as soon as the boom contributes substantially to the blockage (see points 4 and 5 in Fig. 6(a)), the favorable effect of large rotor/fin separation distances is almost annihilated. Second, by comparing the leading (Fig. 6(a)) and trailing edge (Fig. 6(b)) interference, the F/Ts appear to be controlled by the longitudinal position. At equal conditions, the trailing edge localization shows a larger F/T. Minor at low S/A, with growing blockage ratio the penalty can be as high as 50 %. The divergence equates with

(4) $F/T_{\text{trailing edge}} = F/T_{\text{leading edge}} + 0.22\,S/A - 0.033.$

To the authors' best knowledge the location dependence is not reported on up to date. What is more, inversing the direction of rotation from BA to
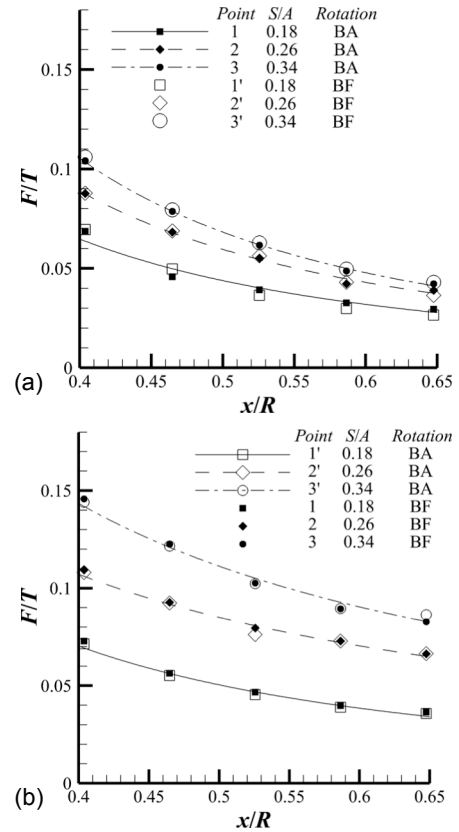

Fig. 7: High tail pusher F/T: (a) leading edge/BA - trailing edge/BF; (b) leading edge/BF - trailing edge/BA

BF (Fig. 7), the combinations position/direction of rotation: leading edge/BA - trailing edge/BF (Fig. 7(a)) and leading edge/BF - trailing edge/BA (Fig. 7(b)); are observed to overlie. Combining those observations allows complementing the early findings by [1]. A first generic tail rotor/fin interference model having the longitudinal position along the vertical fin and direction of rotation as a part in addition to x/R and S/A is proposed in Fig. 8.
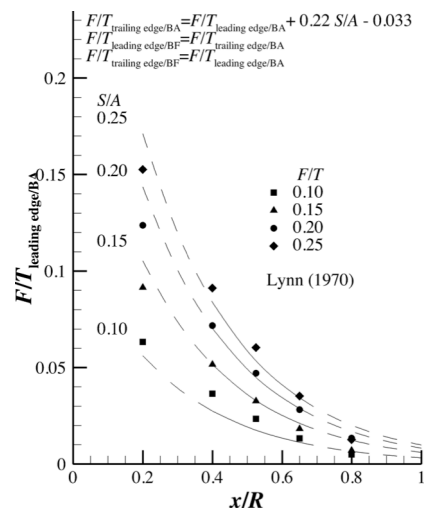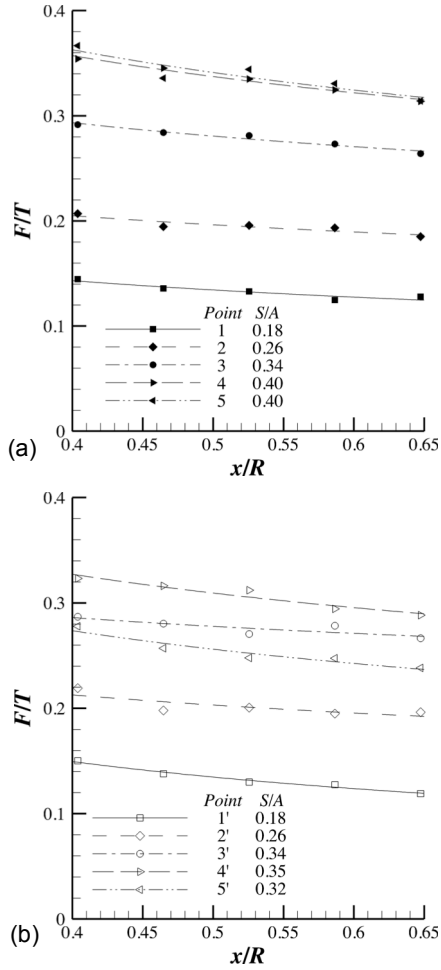

Fig. 8: High tail pusher F/T model

(a)

(b)

Fig. 9: High tail tractor/BA F/T: (a) leading edge; (b) trailing edge

The best-fit mathematical formulation is given by

$$(5) \qquad F/T = \frac{-0.47 S/A^2 + 0.33 S/A - 0.016}{0.11 e^{3.57 x/R}}.$$

To make a comparison with the data in [1] possible, the experimental F/Ts are arithmetically reduced by Equation (5) to accessible S/As from 0.10 to 0.25. The interference map inside and outside the experimented x/R values are depicted in solid and dashed lines respectively. The presented and found data by [1] are seen to correlate qualitatively. Unfortunately, as no longitudinal position data is made available in [1], a quantitative correlation with respect to location dependency as proposed in Equation (4) is inconvenient. To consolidate the projected model, measurements at intermediate longitudinal positions, lying in between the vertical fin leading and trailing edge, are ongoing.

The thrust interference ratios for the tractor arrangement for all measuring points in BA rotational sense are represented in Fig. 9. The leading and trailing edge location data are depicted in Fig. 9(a) and (b) respectively. Overall, similar characteristics to the observations by [1] show up. Compared to the
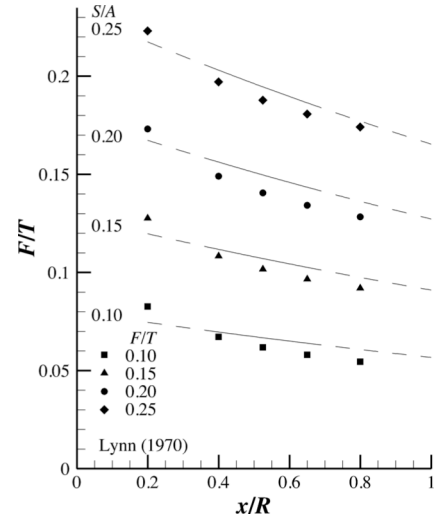

Fig. 10 High tail tractor F/T model

pusher constellation (Fig. 8), on the one hand, the tractor installation is seen to suffer from a higher interference at alike geometrical x/R and S/A conditions. On the other hand, the influence of x/R is seen to be less pronounced. More specific, first, examining the fore and aft position F/Ts in Figs. 9(a) and (b), the longitudinal location appears to have no effect. As such, even in the absence of BF direction of rotation experimentations, by parallelism with the pusher observations, an influence relying on the direction of rotation is also highly improbable. Second the boom interference observed for the measuring points 4 and 5 in close proximity to the boom in pusher leading edge/BA layout (Fig. 6(a)) seem subordinate. Likewise the pusher exercise, the experimental data was fitted:

$$(6) \qquad F/T = \frac{0.42 S/A^2 + 0.65 S/A - 0.007}{0.78 e^{0.34 x/R}},$$

and reduced to installation characteristics made available in [1]. The graphical representation is given in Fig. 10. As for the pusher, the former and present recordings are in line.

Supplementary experimentation is planned in the near future to understand the dissimilar flow effect on the pusher and tractor concepts, i.e. the manifest direction of rotation and location dependency when the fin slows the inflow in pusher set-up, and the free from direction of rotation and location control when the wake blows on the fin in tractor set-up. The apparently highly three-dimensional flow field and coinciding aerodynamical vertical fin/rotor behavior will be studied by three-dimensional Particle Image Velocimetry and pinpointed time resolved velocity measurements by Laser Doppler Velocimetry.

3.1.2. Power interference

For the pusher arrangement, considering the interchangeability of the position/direction of rotation
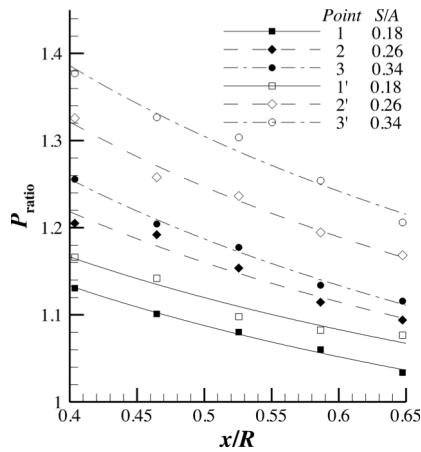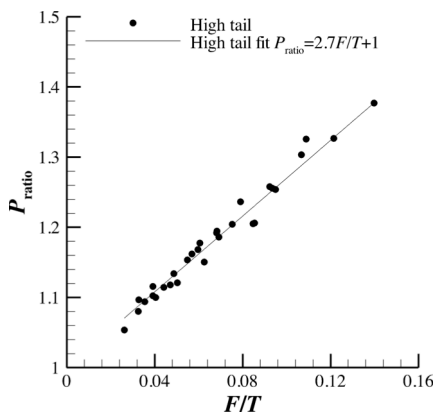
Fig. 11: High tail pusher/BA P_{ratio}

Fig. 12: High tail pusher P_{ratio} as a function of F/T

Fig. 13: High tail F/T and P_{ratio} model

interference (Fig. 12). The chart is to be read as follows: as a function of x/R on the x-axis and parameterized by S/A, F/T on the left hand y-axis applies to leading edge/BA and trailing edge/BF configurations. Leading edge/BF and trailing edge/BA installations are to be adjusted by the expressions in the graph top portion. The P_{ratio} on the right hand y-axis is to be extracted at the actual F/T. Although irrelevant for typical high tail S/As (Table 1), S/A factors outside the parameter range can be obtained by the mathematical formulations in Equations (5) and (7).

For the tractor arrangement, to restrict the experimental effort and considering the F/T reduced efficiency and minor existing implementations, the P_{ratio} was not investigated.

Finally, linking up the location/direction of rotation effects with noise and handling qualities conditions described in Section 1, a trailing edge/BF concept is brought forward as guideline in high tail pusher design. Whereas, at first sight, in high tail tractor design no consideration needs to be given to longitudinal position and sense of rotation.

3.2. Low tail rotor concept

Apparently uncovered in literature, the low tail rotor investigation was directed towards an introductory study. Therefore the experimental scope was restricted to pusher set-up, BA rotational direction and to three longitudinal locations 11 – 13 (see Fig. 5(b) for location reference). In contrast to the high tail concept, the low tail design features a continuous boom, ventral and dorsal fin interaction as schematized by the dashed rotor circumference in Fig. 5(b). One notes the light S/A decrease moving longitudinally from front to vertical fin end.

The F/Ts are represented in Fig. 14. On the one hand, F/T is seen to drop off about linearly with x/R.

pairs, the rotational sense was just set to BA. The P_{ratio} is plotted for the location points 1 – 3 and 1' – 3' (see Fig. 5(a) for location reference) in Fig. 11. As foreseen by the F/T trend (Fig. 6), on the one hand, for both, leading and trailing edge positions, the P_{ratio} goes up with smaller x/Rs and higher S/As. On the other hand, the increment in power to compensate for the trailing edge F/T penalty is brought forward by the horizontal shift in between fore and aft locations at identical S/As (1-1', 2-2' and 3-3'). To check for a P_{ratio} and F/T correlation, the two are plotted against each other in Fig. 12. The F/Ts were computed by Equation (5) for the respective x/R and S/A pairs and afterwards corrected for the position/direction of rotation effect by the reciprocal relations in Fig. 8. An almost linear trend

(7) $$P_{ratio}=2.7F/T+1$$

in between P_{ratio} and F/T shows up. Anticipating an exponential growth with increasing F/Ts, the variance can possibly be attributed to a more pronounced pseudo ceiling effect with increasing F/Ts [6]. What is more, the linear tendency in between P_{ratio} and F/T allows to bring forward an overall tail rotor/vertical fin interference chart in Fig. 13, combining the thrust (Fig. 8) and power
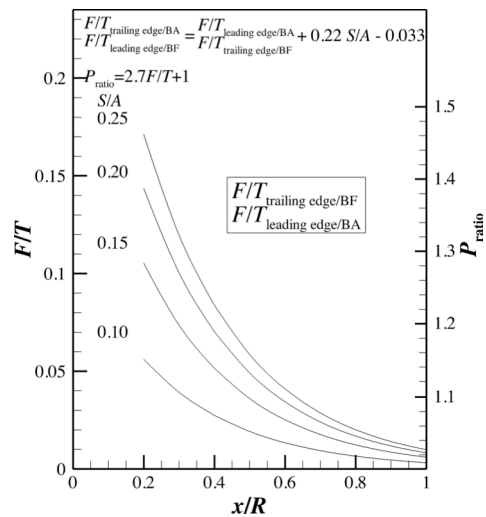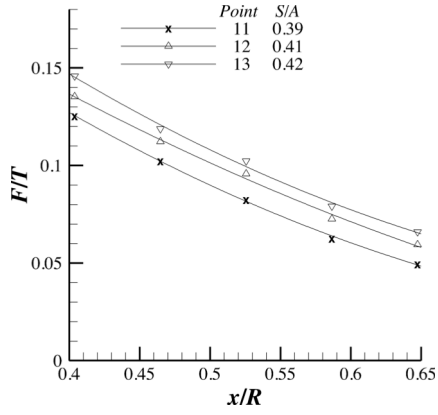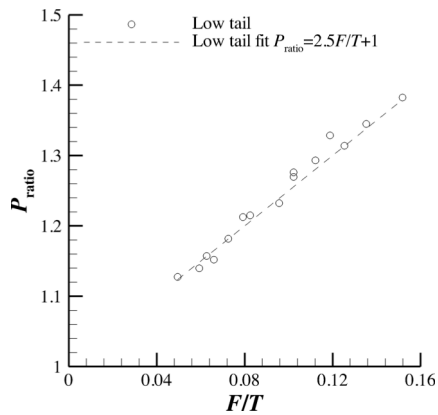
Fig. 14: Low tail pusher/BA F/T

Fig. 15: Low tail pusher/BA P_{ratio} as a function of F/T

(a)

(b)

Fig. 16: Comparison of ventral/dorsal and undivided high fin design in low tail rotor pusher/BA installation: (a) F/T; (b) P_{ratio}

On the other hand, a shift towards lower F/Ts from leading to trailing edge is observed. Considering the negative and positive correlation with respect to fin location/sense of rotation and S/A in the order given, as observed for the pusher/BA configuration (Fig. 6), the F/T dependence seems S/A controlled only. To answer unequivocally the parameter influence and to propose a trustworthy model, testing in both rotation directions, BA and BF, at varying S/As is required. The experimentation is scheduled in the near future.
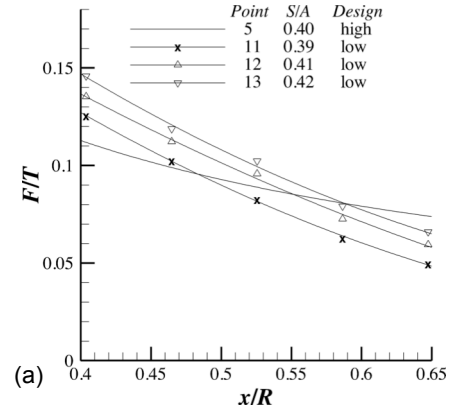
The P_{ratio} as a function of the experimental F/Ts is shown in Fig. 15. As for the high tail (Fig. 12) an almost linear relationship
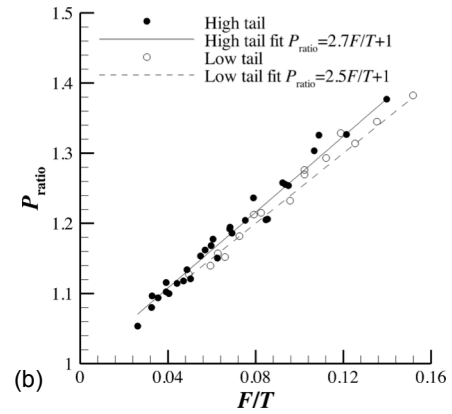
(8) $$P_{ratio}=2.5F/T+1$$

is observed.

3.3. High & low tail rotor concept comparison

To examine the influence on low tail rotors of regularly observed ventral and dorsal fins in combination, as opposed to undivided high fin layouts, both configurations are compared in Fig. 16. In Fig. 16(a) the low (Fig. 14) and high tail (Fig. 6(a)), at approximately equivalent S/As (see point 5 at boom height in Fig. 6(a)), F/Ts are drawn on top of each other. The P_{ratio}s are examined in

Fig. 16(b) by combining the high (Fig. 12) and low (Fig. 15) tail data. In Fig. 16(a) low values of x/R are seen to handicap adequate F/Ts in ventral/dorsal tail design, whereas fin/rotor separation distances above 0.475 exhibit a substantial gain. To take full benefit of the F/T reversal with growing x/R and despite the allowed freedom in tail rotor axis length, off centring the vertical fin with respect to the tail boom is a worthy design option. In addition, it is seen in Fig.16(b) that the ventral/dorsal arrangement also benefits from a slightly inferior P_{ratio}. Mindful of the ventral/dorsal arrangement potential towards larger x/Rs, the future low tail model experimentations will be extended with ventra/dorsal fin surface ratios.

The above considerations only hold for equal S/As, i.e. low tail rotor ventral/dorsal and undivided high tail designs. To compare high and low tail rotor locations, existing arrangements need to be considered. Consulting Table 1, (0.4, 0.2) and (0.5, 0.4) appear representative pairs of (x/R, S/A) for high and low tail concepts respectively. Assuming optimal design, the high tail ($F/T=0.07$, $P_{ratio}=1.19$) is to a small degree superior to the low tail ($F/T=0.09$, $P_{ratio}=1.23$) concept. Although attractive at first sight, the reduced thrust interference and power required are counterbalanced by higher weight and complexity.

4. CONCLUSIONS

The paper presents an experimental study of tail rotor and fin interference in hover and in the absence of a main rotor. A high and a ventral/dorsal low tail design are investigated on a model rotor. For the high tail conception in tractor configuration previous observations are substantiated. By contrast, in pusher configuration, besides early-identified factors, the fin/rotor separation distance and fin area/disc area, the direction of rotation and tail rotor longitudinal position appear to control the interference. The connected power increment was observed to scale with the thrust interference ratio. Accordingly, a widened parametric model is proposed. In addition, linking up the location/direction of rotation effects with noise and handling qualities conditions, a trailing edge/BF concept is brought forward as guideline in high tail pusher design. For the low tail conception, on the one hand, low values of the fin/rotor separation distance are seen to handicap adequate thrust interference ratios as compared to an undivided high tail constellation. On the other hand, with growing tail rotor/fin spacing, the trend reverses and a substantial gain shows up. In addition, the ventral/dorsal arrangement is seen to benefit from a slightly inferior power required. Aware of the limited freedom in tail rotor axis length, off centring the vertical fin with respect to the tail boom is a worthy design option. Finally, the vertical fin top installed tail rotor design was seen to be to a small degree superior to the low tail concept. Although attractive at first sight, the reduced thrust interference and power required are counterbalanced by higher weight and complexity.

5. REFERENCES

[1] R. R. Lynn, F. D. Robinson, N. N. Batra, J. M. Duhon, Tail rotor design guide, Part I – Aerodynamics, Journal of the American Helicopter Society, Vol. 15, No 4, 1970

[2] W. Wiesner, G. Kohler, Tail rotor design guide, USAAMDRL TR 73-99, 1974

[3] R. P. Menger, T. L. Wood, J. T. Beieger, Effects of aerodynamic interaction between main and tail rotors on helicopter hover performance and noise, NASA-CR-166477, 1983

[4] J. W. Leverton, Reduction of helicopter noise by use of a quiet tail rotor, Paper No 24, 6th European Rotorcraft Forum, 1980

[5] R. W. Prouty, Development of the empennage configuration of the YAH-64 advanced attack helicopter, USAAVRADCOM TR 82-D-22, 1983

[6] R. W. Prouty, Helicopter performance, stability, and control, Florida, Krieger Publishing Company, 1995

[7] J. M. Drees, W. P. Hendal, Airflow patterns in the neighborhood of helicopter rotors, Aircraft Engineering, Vol. 23, 1951

[8] D. W. Boatwright, Measurements of velocity components in the wake of a full-scale helicopter rotor in hover, USAAMRDL TR 72-33, 1972

[9] D. R. Clark, Can helicopter rotors be designed for low noise and high performance?, AHS 30th Forum, 1974

[10] A. J. Landgrebe, An analytical and experimental investigation of helicopter rotor hover performance and wake geometry characteristics, USAAMRDL TR 71-24, 1971

6. COPYRIGHT STATEMENT